metals

MDPI

Article

Enhanced Coal Fly Ash Desilication Using Atmospheric NaOH Leaching with Simultaneous Magnetic Separation

Andrei Shoppert [1,*], Dmitry Valeev [2], Irina Loginova [1], Leonid Chaikin [1] and Jinhe Pan [3]

[1] Department of Non-Ferrous Metals Metallurgy, Ural Federal University, 620002 Yekaterinburg, Russia; i.v.loginova@urfu.ru (I.L.); l.i.chaikin@urfu.ru (L.C.)
[2] Laboratory of Sorption Methods, Vernadsky Institute of Geochemistry and Analytical Chemistry of the Russian Academy of Sciences, 119991 Moscow, Russia; dmvaleev@yandex.ru
[3] Key Laboratory of Coal Processing and Efficient Utilization, Ministry of Education, School of Chemical Engineering and Technology, China University of Mining and Technology, Xuzhou 221116, China; jiinhepan@cumt.edu.cn
* Correspondence: a.a.shoppert@urfu.ru

Abstract: Coal fly ash (CFA) is a technogenic waste formed during coal combustion in thermal power plants (TPPs). The extraction of valuable components from CFA is complicated by the presence of a large amount of amorphous glassy mass and iron. Herein, a novel method of CFA desilication with complete extraction of the amorphous glassy mass without desilication product (DSP) precipitation and simultaneous magnetic fraction recovery in one stage is presented. The Fe recovery in the magnetic fraction using the proposed method was significantly improved from 52% to 68%. After conventional wet magnetic separation, followed by the proposed method for desilication and magnetic fraction separation, the Fe recovery was increased to 73.8%. Because of the absence of DSP precipitation, the Na_2O content in the solid residue after desilication was lower than 1 wt.%. The simultaneous desilication and magnetic separation of magnetite was achieved by installing a belt of permanent magnets on the outer surface of the reactor, where the CFA was leached by the highly concentrated NaOH solution. The effects of different parameters on the extraction of Si, Al, and Fe from the raw CFA were elucidated by varying the liquid-to-solid ratio (L:S ratio) from 5 to 10, the temperature from 100 to 120 °C, the leaching time from 10 to 30 min, and the particle size from −50 µm to −73 µm. The optimal leaching parameters were determined to be temperature = 110 °C, L:S ratio = 7.5, and leaching time = 20 min. The extraction of Si and Fe under these conditions was higher than 66 and 73%, respectively. The Al extraction was lower than 10%. The solid residue of NaOH leaching and the magnetic fraction were examined by X-ray diffraction, X-ray fluorescence spectrometry, vibrating sample magnetometry, scanning electron microscopy with energy-dispersive X-ray spectroscopy, Brunauer–Emmett–Teller, and laser diffraction analyses.

Keywords: coal fly ash; alkaline leaching; iron extraction; kinetics; desilication; waste utilization

Citation: Shoppert, A.; Valeev, D.; Loginova, I.; Chaikin, L.; Pan, J. Enhanced Coal Fly Ash Desilication Using Atmospheric NaOH Leaching with Simultaneous Magnetic Separation. *Metals* **2023**, *13*, 1647. https://doi.org/10.3390/met13101647

Academic Editor: Antoni Roca

Received: 25 August 2023
Revised: 19 September 2023
Accepted: 24 September 2023
Published: 25 September 2023

1. Introduction

Coal fly ash (CFA) is the most-abundant waste produced during coal combustion worldwide. CFA formation is estimated to reach 2.2-billion t by 2025 [1,2]. The construction industry can consume 30–70% of the CFA, depending on the country [3–5]. The remaining CFA is disposed in landfills, thus causing severe environmental pollution [6–8]. CFA contains high amounts of valuable components (such as Si, Al, Fe, and REEs), which can be extracted using alkaline or acidic methods [9–11]. However, the high amount of silica in the CFA presents technological challenges in terms of its chemical treatment. However, an alumina/silica ratio (μ_{Si} = Al_2O_3/SiO_2) above 1 renders the alkaline method of Al extraction economically unfeasible [12,13]. Thus, acidic methods for CFA treatment have recently been extensively studied [14–16]. The presence of valuable components in the solid matrix of most refractory aluminosilicate–mullite formed during coal combustion at

temperatures higher than 1200 °C requires high-pressure leaching [17,18] or preliminary activation [19–21].

The preliminary treatment of CFA, such as desilication and magnetic fraction extraction, is suitable, enriching the valuable components in the CFA and reducing the reagent consumption and temperatures of the leaching [22,23]. Using the desilication method, silicon (Si) from an amorphous glassy mass that accounts for almost half of the mass of the CFA is extracted into an alkaline solution, whereas Al, Fe, and REEs are enriched in the solid residue [24–26]. The primary drawback of this method is the formation of the sodalite desilication product (DSP) ($Na_6[Al_6Si_6O_{24}]$ NaX, where X represents various inorganic anions, which are primarily sulfate, carbonate, chloride, and aluminate) [13]. DSP precipitates when Al and Si are present together in an alkaline solution. Owing to the DSP precipitation, the solid residue Na_2O content can reach 12–14 wt.% [15,27]. Thus, to reduce the amount of sodalite in the solid residue, the preliminary acid extraction of the soluble Al before desilication is suggested [28]. The use of the acid–alkali–acid leaching method was reported by [29,30]. However, such methods have numerous washing steps, and the inevitable neutralization of the acid and alkali cannot be avoided.

Another viable method for CFA enrichment is magnetic separation, which helps extract more than half of the Fe contained in the CFA in the form of magnetite [31,32]. Furthermore, research has revealed that REEs in CFA are enriched in the aluminosilicate phase [33,34], and magnetite extraction helps increase the REE concentration in the nonmagnetic fraction. Commonly, wet [35] or dry [36] magnetic separation is used to extract the magnetite from the CFA before leaching. Nonetheless, the recovery of iron in the magnetic concentrate using these methods is less than 60–70% [37] because some Fe is present as hematite and some parts of the magnetite are encapsulated in the aluminosilicate solid matrix.

Our previous research demonstrated that, by varying the leaching time and the concentration of the NaOH solution, Si can be maintained in the solution during preliminary desilication [22]; consequently, the formation of sodalite was avoided. However, the primary disadvantages of this method are the high L:S ratios and co-dissolution of easily soluble Al (up to 35 wt.%). In this study, the possibility of further reducing the L:S ratio of the process without sodalite formation was investigated by combining desilication with magnetic separation. In addition, the effects of different leaching parameters (temperature, L:S ratio, time, and particle size) of pulverized coal (PC) furnace fly ash desilication using a highly concentrated NaOH solution and permanent magnet field were investigated for the first time. The solid residue obtained by the novel desilication technique was enriched with Al and REEs, which are associated with the uncovered mullite agglomerates and can be easily extracted by acid leaching with an extraction degree higher than 60–70% at atmospheric pressure [12]. The low concentration of Na_2O and Fe in this residue significantly reduced the acid consumption. The chemical and phase compositions of the solid residues obtained via the novel desilication method were analyzed using X-ray diffraction (XRD), X-ray fluorescence spectrometry (XRF), and scanning electron microscopy, with energy-dispersive X-ray spectroscopy (SEM-EDX). The physical properties of the residue were examined using a vibrating sample magnetometer (VSM), the Brunauer–Emmett–Teller (BET) method, and the laser diffraction (LD) method.

2. Materials and Methods

2.1. Raw Materials

The CFA used in these experiments was obtained from the Reftinskaya thermal power plant in Asbest, Russia (GPS coordinates: 56.11° N, 61.70° W). Before the leaching experiments, the raw CFA was subjected to a screening test. The chemical compositions of the four size fractions of the CFA are listed in Table 1. Table 1 indicates that all the size fractions had similar chemical compositions. However, the coarse particle size fraction had a low amount of iron, and the smallest particle size fraction had the highest contents of alumina and iron, which could be related to the lowest concentration of the amorphous glassy mass. The lowest concentrations of Na_2O and K_2O in the −50 μm-sized fraction confirmed that

these oxides were associated with aluminosilicates [38–40]. Figure 1 shows the XRD pattern of the raw CFA.

Table 1. Chemical composition of the three size fractions of the raw coal fly ash (CFA) from the Reftinskaya TPP.

Product	Components (wt.%)										
	SiO_2	Al_2O_3	CaO	Fe_2O_3	FeO	TiO_2	MgO	Na_2O	K_2O	LOI *	C
−50 µm	59.89	26.79	1.60	2.63	1.10	1.11	0.43	0.57	0.82	3.99	1.90
−61 µm	62.73	24.31	1.63	2.27	1.04	1.09	0.44	0.68	0.91	3.90	1.78
−73 µm	62.43	24.66	1.60	2.29	1.05	1.12	0.43	0.72	0.94	3.70	1.60
+73 µm	63.87	24.27	1.84	1.56	0.68	0.82	0.53	0.76	0.90	3.60	1.60

* LOI—loss on ignition at 1000 °C.

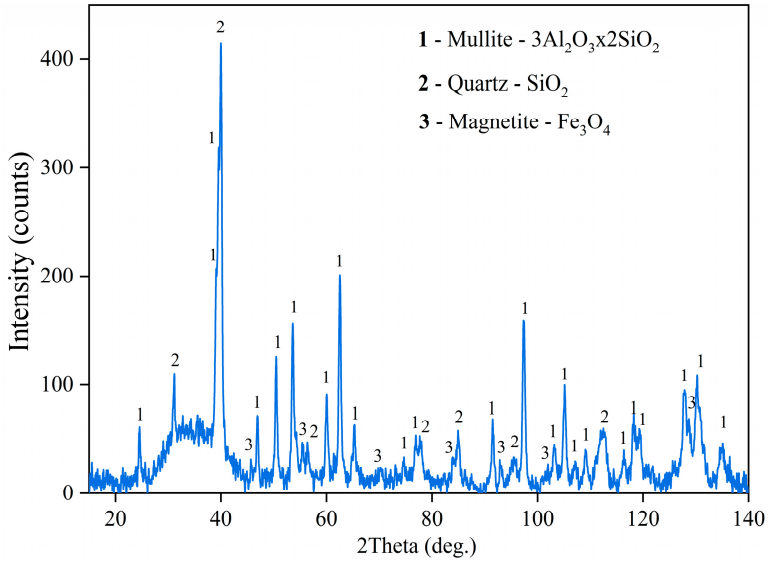

Figure 1. XRD pattern of the raw CFA from the Reftinskaya TPP, Russia.

Evidently, the raw CFA consisted of an amorphous glassy mass (with the halo ranging from 20° to 50°), mullite, quartz, and a low amount of magnetite. However, according to Table 1, some Fe was present in the raw CFA as hematite because the stoichiometric amount of FeO in the Fe_3O_4 was 31%. For example, according to the stoichiometry, the amount of Fe_2O_3 in magnetite should be 2.45 wt.%, not 2.63 wt.%. The morphology and chemical composition of the CFA particles were determined by SEM-EDX analysis (Figure 2). As shown in Figure 2d, the raw CFA consisted of spherical particles, with a high amount of aluminum and silicon, and a smooth surface. Therefore, the mullite was more likely to be covered by amorphous aluminosilicate. Additionally, irregular particles (Figure 2b,d) with a high amount of Si, an amorphous glassy mass, and quartz were observed. Other analytical-grade chemical reagents were used in this study.

2.2. Experimental Procedure

The CFA was leached with NaOH in a 0.5 L thermostated reactor equipped with a neodymium magnet (magnetic field strength, 0.6 T; dimensions, 10 mm × 5 mm × 2 mm; Forceberg, Moscow, Russia) belt (Figure 3), which simultaneously enabled the separation of iron. This reactor had an opening for stirring and allowed controlling the temperature and recycling evaporated water through a water-cooled condenser.

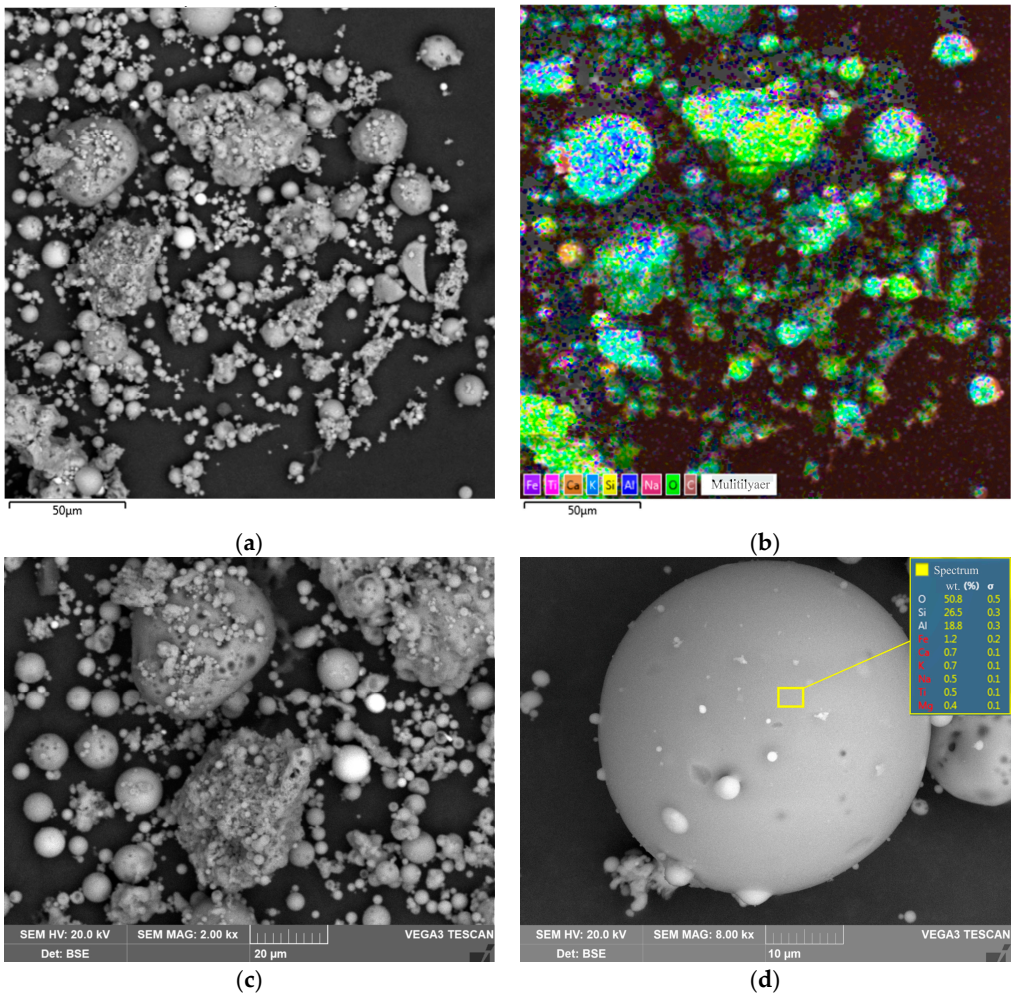

Figure 2. SEM-EDX images of raw CFA: (**a**) backscattered electron (BSE) image of the particles' surface at a magnitude of 1000×; (**b**) mapping of the elemental composition of the surface of the particles in Figure 2a; (**c**) BSE image of the particles' surface at a magnitude of 2000×; (**d**) BSE image of a mullite spherical particle with the result of the EDS analysis.

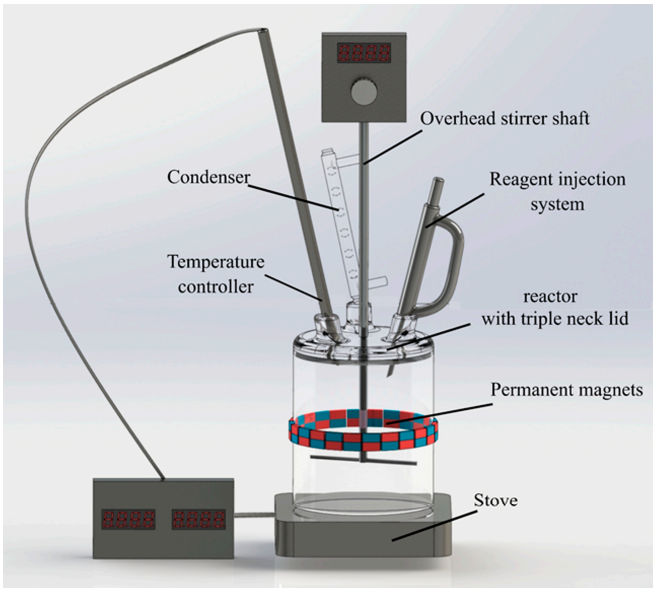

Figure 3. Experimental setup for CFA leaching by NaOH with simultaneous magnetic separation.

All the experiments were conducted at a stirring speed of 300 rpm. The raw CFA was added to an alkaline solution with a concentration of 330 g L^{-1} Na_2O, which enabled using the atmospheric leaching process at a temperature of up to 120 °C and higher. Our previous research [22] demonstrated that further increases in the concentration of the solution did not lead to a significant enhancement of the Si extraction. The L:S ratio (L:S) was varied from 5 to 10; the temperature of the leaching (T) was varied from 100 to 120 °C; the leaching time (τ) was varied from 10 to 30 min; the particle size fraction (r_0) ranged from −50 μm to −73 μm. Different particle size fractions of the CFA were obtained using a vibratory screening machine (PE-6700, ECROS, Saint-Petersburg, Russia). After leaching, the pulp was filtered, and the solid residue was dried at 110 °C for 8 h before analysis.

To avoid the mutual influence of factors and reduce the number of experiments, a Box–Benken plan was constructed using the "Statistica" software version 13 (TIBCO, Hamburg, Germany). This plan included three blocks of 27 experiments with the varying of the parameters at three levels. The output parameters were the extraction of aluminum and silicon into the solution, the extraction of iron into the magnetic fraction, and the content of Na_2O in the solid residue.

A statistical-based automated neural network (SANN) was used to model the CFA leaching using NaOH. A multilayer perceptron (MLP) approach was employed for the SANN modeling in the Statistica 13 software. The best SANN model for the description of the CFA leaching was MLP with $R^2 = 0.98$ and the configuration 4.20.4, where 4 is the number of input parameters, 20 is the number of hidden layers, and 4 is the number of output layers.

2.3. Analysis

The chemical compositions of the raw CFA and residues after leaching were analyzed using powder XRF with an Axios MAX spectrometer (Malvern Panalytical Ltd., Almelo, The Netherlands). Tablet-shaped samples (diameter, 20 mm; mass, 300 mg) were prepared for analysis via pressing, and polystyrene was used as a binder at a ratio of 5:1. The metallic contents of the samples were calculated using the Super Q V.4 software.

The phase compositions of the raw CFA and residues after leaching were analyzed by XRD using a Difrei-401 diffractometer (JSC Scientific Instruments, Saint Petersburg, Russia) with a Cr-Kα radiator for 2θ angles ranging from 15° to 140°. The X-ray source was operated at an output of 25 kW and an exposure time of 30 min. The diffraction data were processed using the Match 3! software version 3.15 (Crystal Impact GmbH, Bohn, Germany). The surface morphology and elemental mapping of the raw materials and residues were investigated using SEM-EDX on a Vega III microscope (Tescan, Brno, Czech Republic). The particle size distribution of the raw CFA and the products of leaching was measured using the laser diffractometer Bettersizer ST (Bettersize Instruments Ltd., Dandong, China). The specific surface area (BET method) was analyzed using a NOVA 1200e (Quantachrome Instruments, Boynton Beach, FL, USA). Magnetic field calculations were performed using finite-element modeling in SolidWorks (Dassault Systèmes, Vélizy-Villacoublay, France). Conventional wet magnetic separation was performed at 0.5 T and a solid concentration of 250 g L^{-1} using an MBSL magnetic separator (NPO Erga, Kaluga, Russia).

The following Equations (1) and (2) were used to calculate the Fe recovery after the wet magnetic separation, simultaneous alkali leaching, and magnetic separation [39].

$$R = (\gamma \times \beta)/\alpha \times 100\%, \quad (1)$$

where R is the recovery of Fe (%); γ is the yield of the magnetic fraction (%); and α and β are the grade of Fe in the raw CFA and magnetic fraction, respectively (%).

$$E = [(R - \gamma)/(100 - \alpha)] \times 100\%, \quad (2)$$

where E is the efficiency index (%). If E > 75%, the enrichment process is highly efficient, if 50% < E < 75%, it is efficient, whereas if E < 25%, it is inefficient [40].

The amounts of Si, Al, and Fe extracted from the CFA (X) into the solution were estimated using Equation (3), as follows:

$$X = (m_1 \times X_1 - m_2 \times X_2)/(m_1 \times X_1), \quad (3)$$

where m_1 is the mass of the original sample (g); X_1 is the elemental content in the original sample (%); m_2 is the mass of the leaching residue (g); and X_2 is the elemental content in the leaching residue (%).

3. Results and Discussion

3.1. Effects of Leaching Parameters on Al, Si Extraction, Fe Recovery, and Na_2O Content in the Solid Residue

Leaching tests with simultaneous iron separation were conducted to determine the effect of different parameters on the Si and Al extraction into solution, the degree of Fe separation into the magnetic fraction, and the content of Na_2O in the solid residue. The experimental data and values predicted using the SANN model were in good agreement (R^2 = 0.98). The response surfaces predicted by the SANN for Si extraction, depending on the leaching duration (τ, min), temperature (T, °C), L:S ratio (L:S), and initial particle size fraction (r_0, μm), are shown in Figure 4.

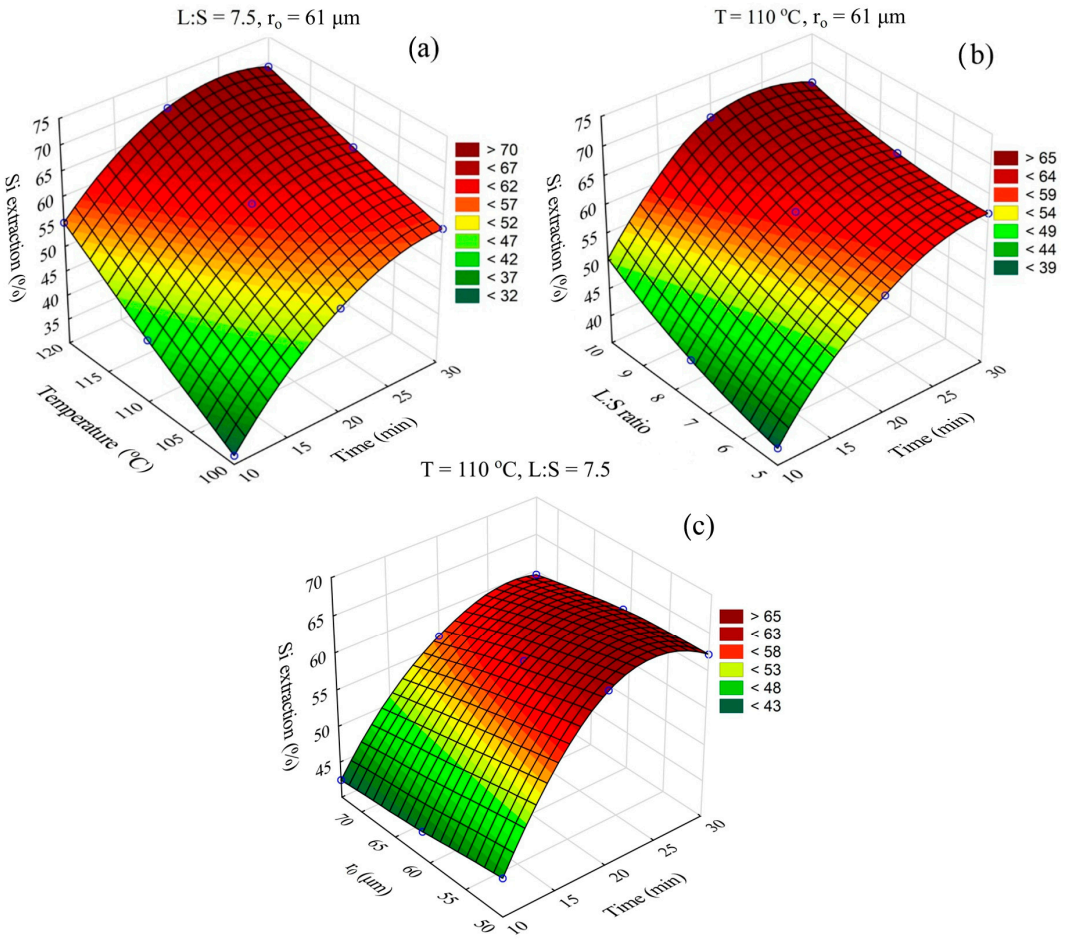

Figure 4. Neural network response surfaces for the effect of: (**a**) time and temperature on the Si extraction; (**b**) time and L:S ratio on the Si extraction; (**c**) time and r_0 on the Si extraction.

Evidently, the Si extraction (Figure 4) was influenced predominantly by the leaching time and temperature. An increase in the temperature from 100 °C to 120 °C led to an increase in the Si extraction from 35 to 55% after 10 min of leaching and from 57% to 70% after 30 min of leaching (Figure 4a). An increase in the L:S ratio from 5 to 10 led to

an increase in the Si extraction by 10% for all leaching durations (Figure 4b). Increasing the r_0 from −50 µm to −73 µm reduced the Si extraction from 62 to 60% after 30 min of leaching (Figure 4c).

Additionally, the Al extraction (Figure 5) was also influenced predominantly by the leaching time and temperature, which can be explained by the dissolution of the amorphous glassy mass contained in the Si and the easily soluble Al [28].

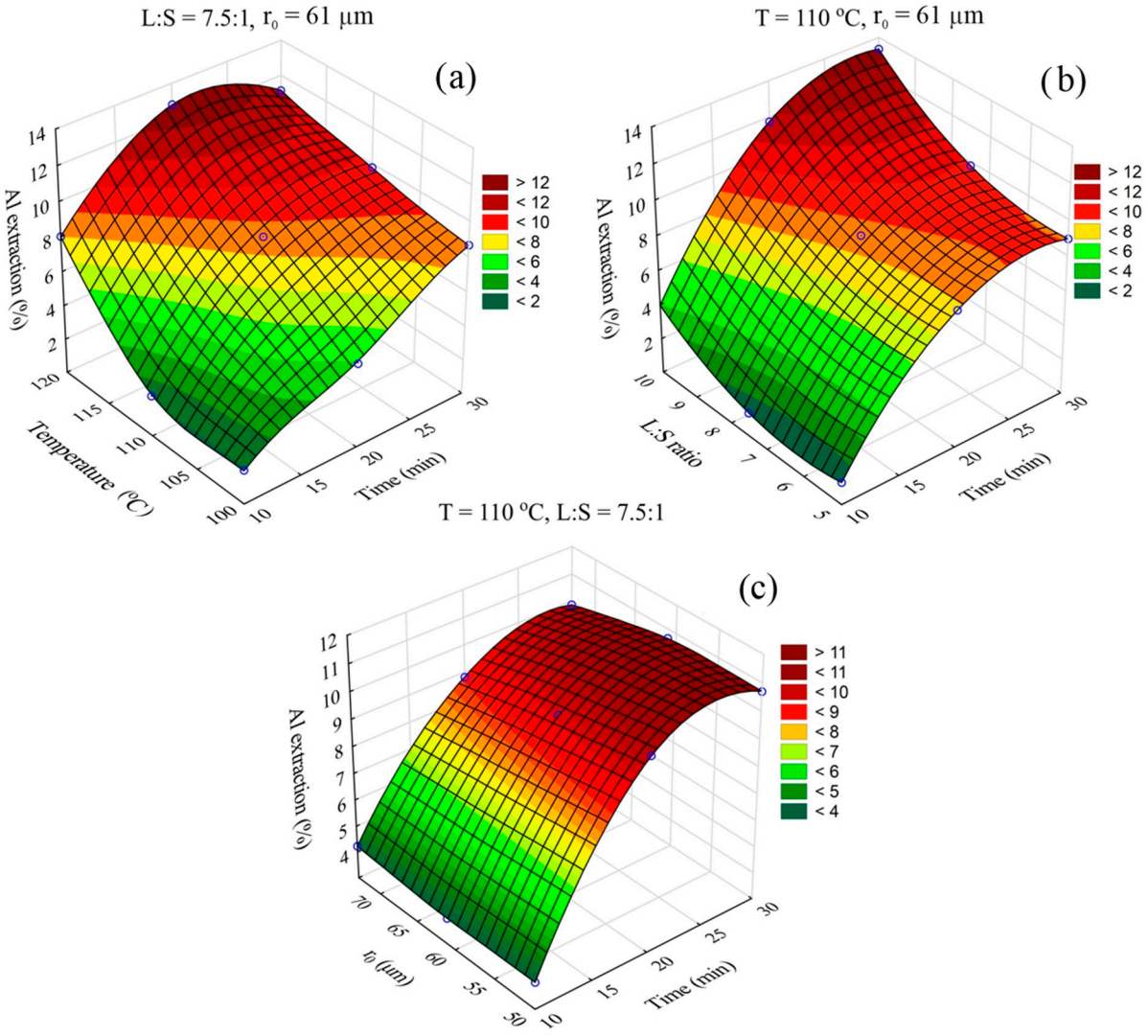

Figure 5. Neural network response surfaces for the effect of: (**a**) time and temperature on the Al extraction; (**b**) time and L:S ratio on the Al extraction; (**c**) time and r_0 on the Al extraction.

Figure 5a shows that, during the first 20 min of leaching at T = 120 °C, the Al extraction degree exhibited an increasing trend. After 20 min of leaching, the Al began precipitating in the form of a desilication product; this was confirmed by the increased content of Na_2O in the solid residue after 30 min of leaching at the higher temperature (Figure 6). However, at the higher L:S ratio (Figure 5b), this phenomenon was absent, which was associated with the retention of Si in the solution. Figure 5c shows that the median particle size had a low effect on the Al extraction. A comparison of Figures 4a and 5a reveals that increasing the Si extraction to higher than 50–60% resulted in an increase in the Al extraction to 10% and higher, and the L:S ratio had a greater effect on the Al extraction than on the Si extraction after 30 min of leaching. This was owed to the fact that the mullite (mineral with the high Al content) began to dissolve.

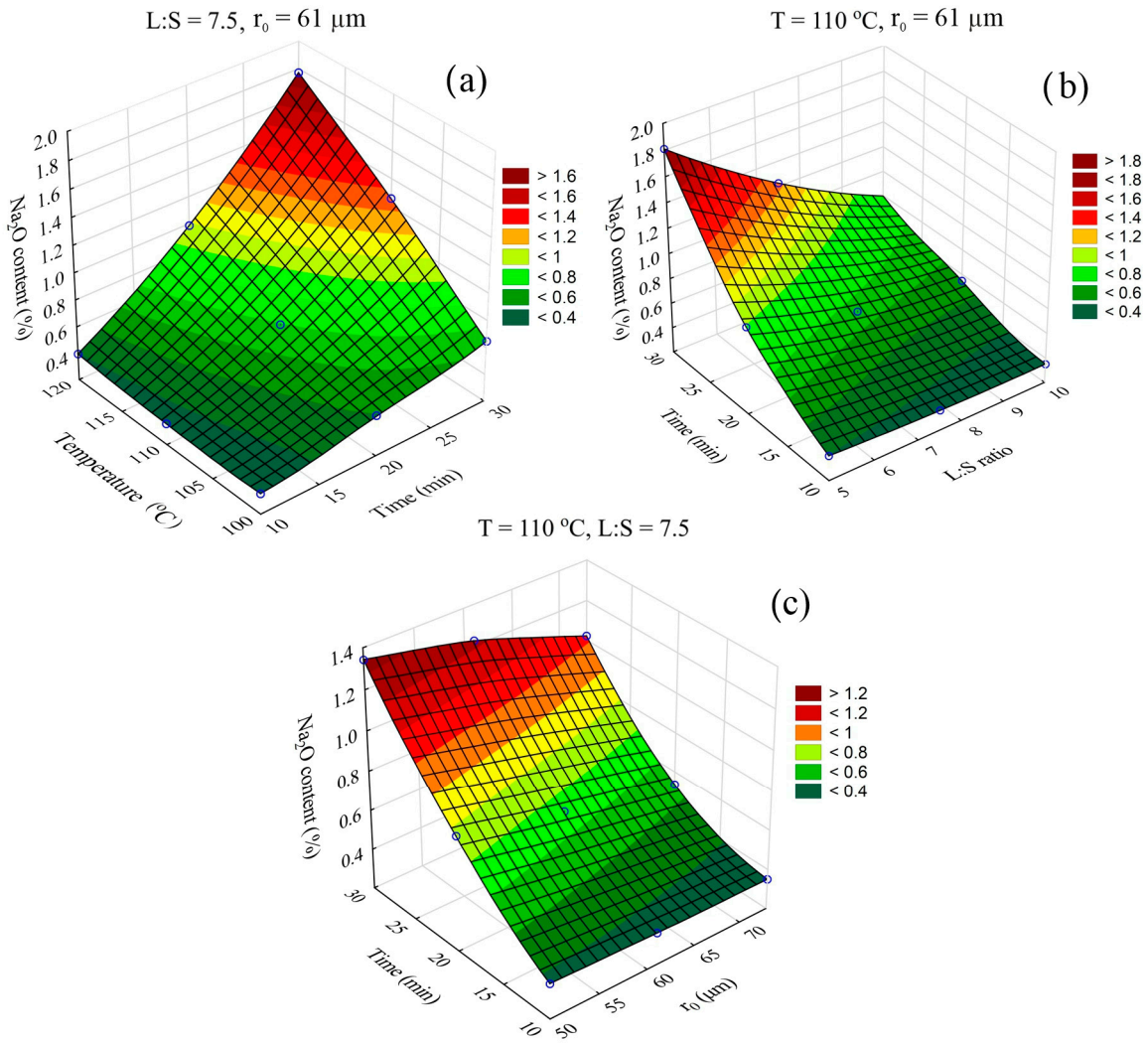

Figure 6. Neural network response surfaces for the effect of: (**a**) time and temperature on the Na_2O content in the solid residue; (**b**) time and L:S ratio on the Na_2O content in the solid residue; (**c**) time and r_0 on the Na_2O content in the solid residue.

Figure 6a,b indicate that, after 30 min of leaching at a low L:S ratio (<7.5) and T > 110 °C, the Na_2O content in the solid residue was higher than 1 wt.%. This indicates that the DSP began to form after the Si and Al concentrations in the solution reached exact values. Furthermore, the effect of r_0 on the Na_2O content in the solid residue was very low (Figure 6c).

The Fe recovery in the magnetic fraction was influenced primarily by leaching time and L:S ratio (Figure 7a–c). This can be related to the dissolution of the amorphous glassy mass from the surface of the magnetic particles and the higher specific surface area of the magnets to the fly ash at high L:S ratios. Increasing the leaching temperature did not lead to an increase in the Fe recovery after 30 min of leaching (Figure 7a). However, it had a significant effect on the Si and Al extraction. This can be related to the dissolution at a later stage of the mullite that did not cover the magnetite particles. The effect of r_0 on the Fe recovery was insignificant. However, the yields of the magnetic concentrates were different: 3.75% for a size fraction of −50 µm and 4.75% for a size fraction of −73 µm. These discrepancies were caused by differences in the chemical compositions of the magnetic fractions, as presented in Section 3.2.

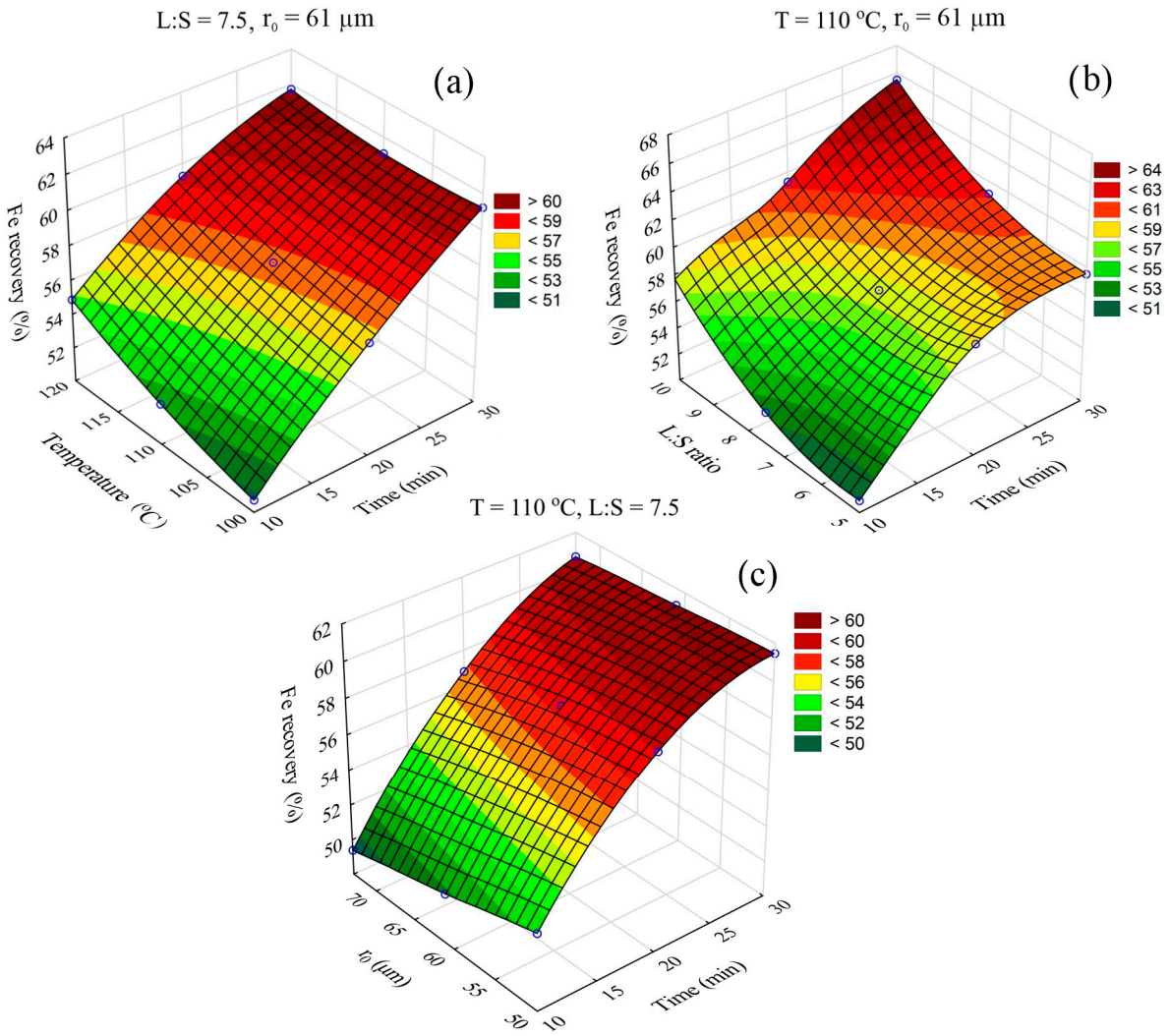

Figure 7. Neural network response surfaces for the effect of: (**a**) time and temperature on the Fe separation efficiency; (**b**) time and L:S ratio on the Fe separation efficiency; (**c**) time and r_0 on the Fe separation efficiency.

According to the results of the leaching parameter effects on the Al and Si extraction, Fe recovery, and Na_2O content in the solid residue, the optimal parameters of the leaching can be suggested as: T = 110 °C, t = 20 min, and L:S = 7.5. At all r_0 values, the Si and Fe extractions were higher than 60%, whereas the Al extraction and Na_2O content in the solid residue were lower than 8% and 1 wt.%, respectively.

3.2. Solid Residue Characterization

Table 2 lists the physical properties of the raw CFA, nonmagnetic fraction, and magnetite concentrate obtained from the CFA −50 µm-sized fraction under optimal conditions. Evidently, from Table 2, the specific surface area, total pore volume, and pore diameter of the leaching products were much higher. The most-distinct changes were observed in the median particle size: after desilication and elimination of the glassy mass from the surface of the particles, the median particle size was considerably reduced, from 28 to 15–16 µm.

Table 2. Physical properties and median particle size of the CFA (size fraction, −50 µm) nonmagnetic fraction and magnetite concentrate obtained during CFA −50 µm-sized fraction leaching at T = 110 °C, τ = 20 min, and L:S = 7.5.

Product	Specific Surface Area (BET) (m^2 g^{-1})	Total Pore Volume (cm^3 g^{-1})	Pore Diameter (nm)	Median Particle Size (µm)
CFA −50 µm-sized fraction	5.70	12.0	15.2	28.30
Nonmagnetic fraction	15.12	28.0	23.5	14.59
Magnetic fraction	11.60	25.0	18.7	16.24

Table 3 presents a comparison of the chemical compositions of the nonmagnetic and magnetic fractions obtained under optimal conditions. Evidently, the Al content in the nonmagnetic concentrates approximately doubled, and a part of the aluminosilicate was captured by the magnetic fraction. Moreover, the Fe content in the magnetic fractions obtained from the −50 µm-sized fraction was much higher. The Fe content in the magnetic concentrate obtained from this type of CFA by conventional magnetic separation did not exceed 20 wt.% [41]. The XRD patterns of the nonmagnetic and magnetic fractions obtained after NaOH leaching of the −50 µm particle size fraction of the raw CFA are shown in Figure 8. Evidently, the magnetic fraction comprised magnetite and hematite, and a low amount of quartz and mullite was entrapped in the concentrate. The nonmagnetic fraction was a desilicated CFA with an amorphous glassy mass (with 2θ ranging from 20° to 50°), and the magnetite was eliminated. In addition, the mullite peaks were higher than those of the quartz, which indicates quartz co-dissolution.

Table 3. Chemical composition of nonmagnetic and magnetic concentrates obtained during desilication of the different particle size fractions of the raw CFA at T = 110 °C, τ = 20 min, and L:S = 7.5.

Product	Major Components (wt.%)									
	SiO_2	Al_2O_3	CaO	Fe_2O_3	TiO_2	MgO	Na_2O	K_2O	LOI *	C
Nonmagnetic fraction −50 µm	37.00	43.04	3.51	2.50	1.92	0.87	0.98	0.08	7.20	2.60
Nonmagnetic fraction −73 µm	40.35	41.77	3.21	2.73	2.03	0.83	0.75	0.13	7.90	2.78
Magnetic fraction −50 µm	14.99	13.59	2.44	62.64	0.53	2.03	1.32	0.05	1.70	0.79
Magnetic fraction −73 µm	21.23	19.92	3.88	48.33	0.81	1.79	1.68	0.08	1.80	0.93

* LOI—loss on ignition at 1000 °C.

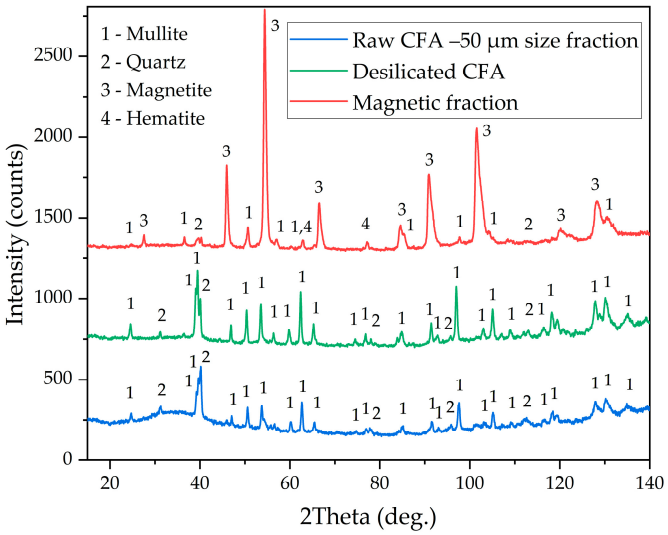

Figure 8. XRD patterns of the magnetic and nonmagnetic fraction and the raw CFA −50 µm-sized fraction.

Figure 9 and Table 4 show that high amounts of Al and Fe in the solid residue were observed after desilication of the −73 µm-sized fraction; this can be attributed to the encapsulation of aluminosilicate in the solid matrix of the magnetic spheres.

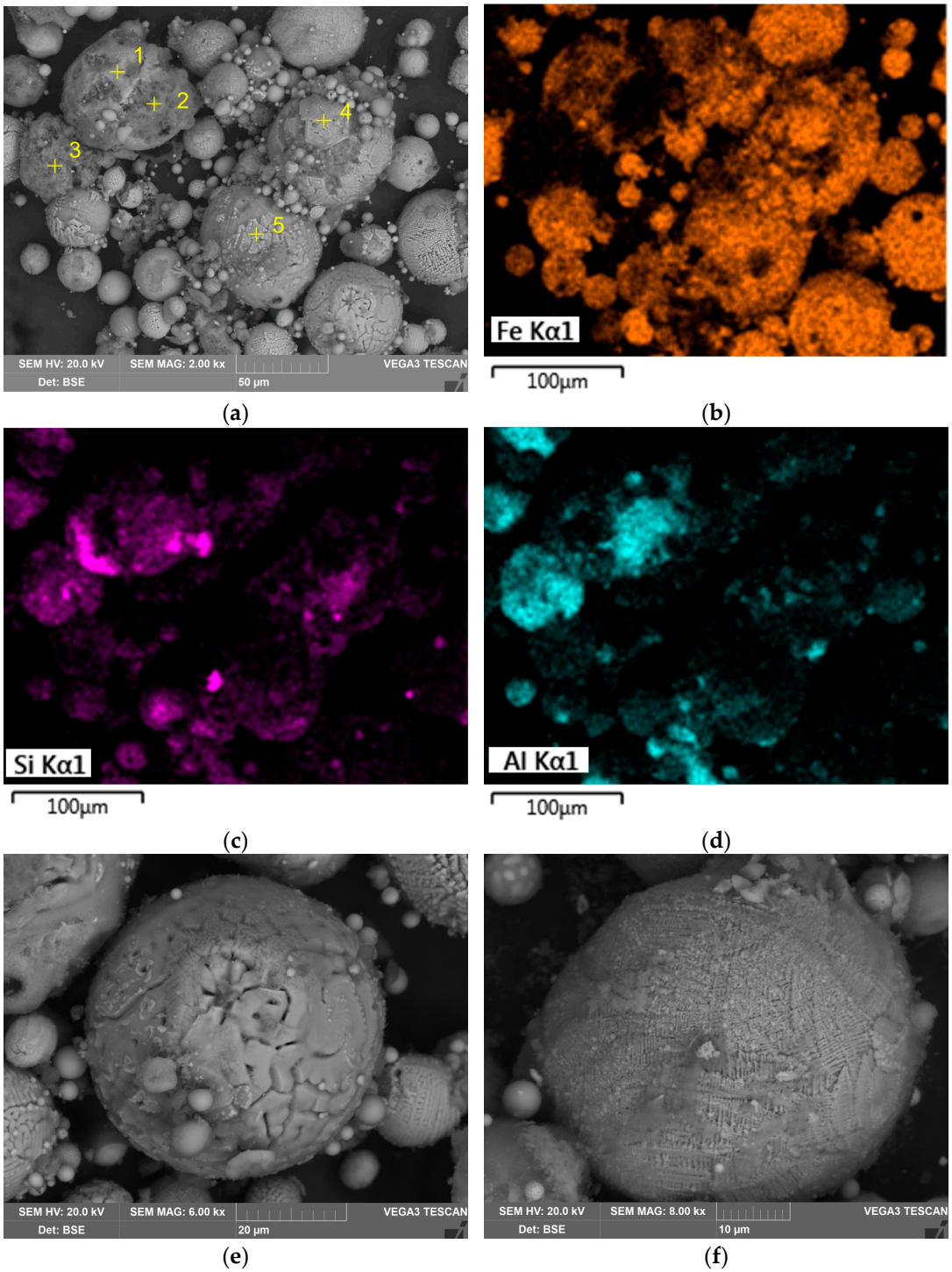

Figure 9. SEM-EDX images of the coarse magnetic fraction: (**a**) BSE image of the particles' surface at a magnitude of 2000× with the EDS points (yellow cross indicates place of EDX analysis, the elemental compositions are shown in Table 4); (**b**–**d**) mapping of the elemental composition of the particles' surface in Figure 9a; (**e**) BSE image of the magnetic sphere's surface at a magnitude of 6000×; (**f**) BSE image of the magnetic sphere's surface at a magnitude of 8000×.

Table 4. Elemental compositions (wt.%) of solid residue particles' surface (listed spectral numbers correspond to the points highlighted in Figure 9a).

Spectral Number	O	Al	Si	Fe	Ti	Ca	Na	Mg	K
1	14.8	5.3	4.2	68.2	2.3	3.8	1.5	-	
2	52.4	24.0	17.7	1.3	0.3	2.1	1.8	0.3	
3	54.6	26.8	14.6	2.0	0.6	1.1	-	-	0.2
4	28.9	1.3	1.1	65.6	-	0.6	-	1.0	-
5	30.9	5.9	4.0	53.6	0.8	2.2	-	1.6	

The SEM-EDX analysis (Figure 9, Table 4) revealed that the aluminosilicate was encapsulated inside the solid matrix (Spectral Number 2 in Figure 9a–d). Additionally, aluminosilicate was physically trapped in the magnetic concentrate (Spectral Number 3). Therefore, a larger particle size resulted in higher aluminosilicate co-extraction with the magnetic concentrate. Consequently, the Fe_2O_3 content in the magnetic fraction obtained after leaching the −73 µm particle size fraction was lower than that of the −50 µm-sized fraction. Figure 9e,f display the morphologies of the magnetic particles.

The SEM-EDX analysis (Figure 10) revealed that, after Si extraction by NaOH leaching at T = 110 °C, t = 20 min, and L:S = 7.5, the acicular mullite particles were exposed, and some of the magnetic particles remained in the nonmagnetic fraction, which indicates incomplete Fe separation. The incompleteness of Fe separation can be explained by the low surface area of the magnets or the weak magnetic field. Thus, the spatial distribution of the magnetic flow of the permanent magnets was evaluated, and a finite-element model of the magnetic field in the reactor was constructed (Figure 11).

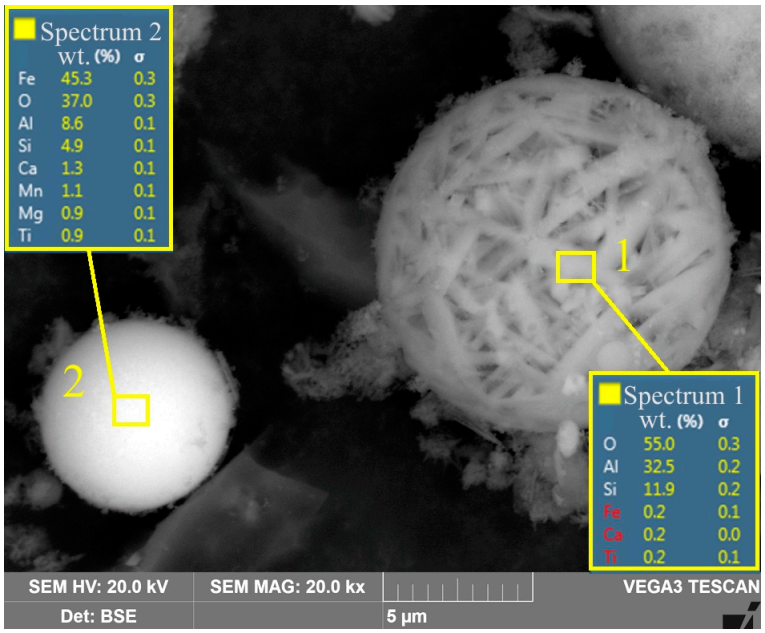

Figure 10. SEM-EDX image of the magnetic sphere surface and mullite agglomerate sphere at a magnitude of 20,000×.

As shown in Figure 11, the magnetic field did not extend deeply into the reactor. The proposed permanent magnet design resulted in the capture of particles located directly near the reactor wall. To overcome this shortcoming, the magnetic belt design will be enhanced in future research, thus allowing harmonization of the flows.

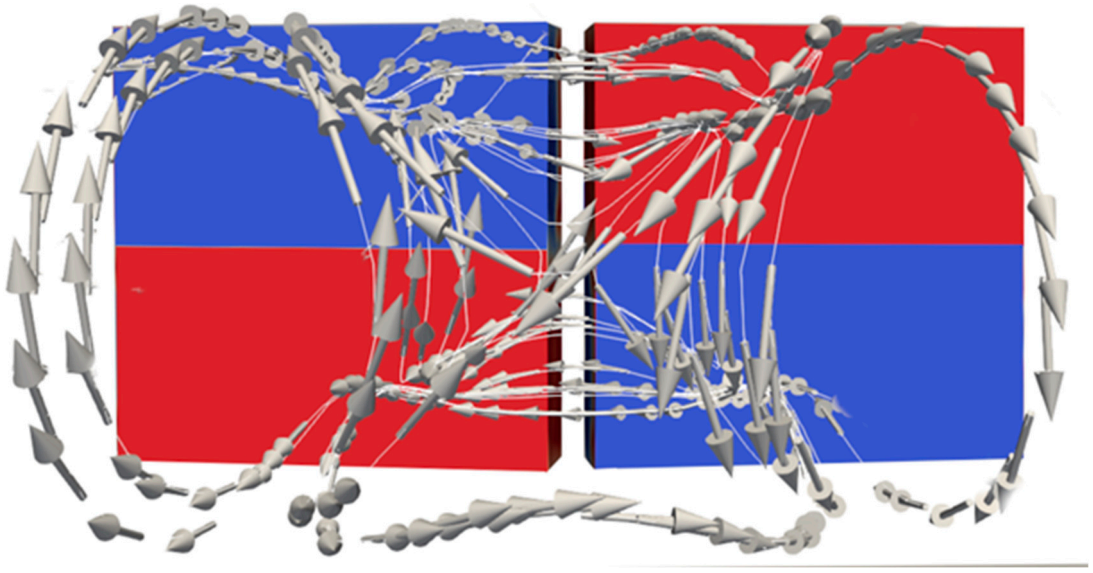

(**a**)

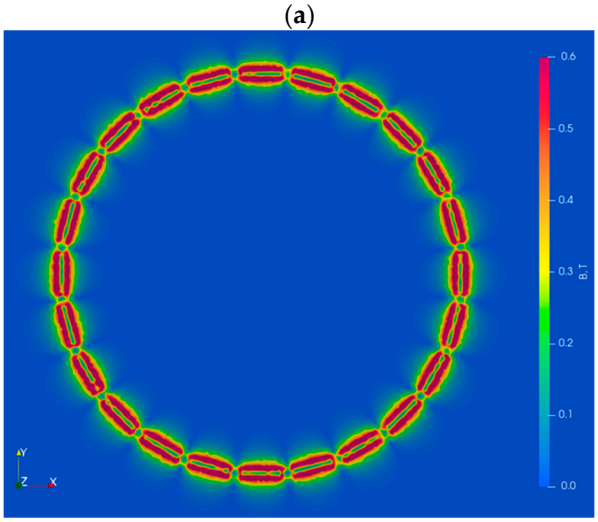

(**b**)

Figure 11. Result of the finite-element modeling of the spatial distribution of the magnetic field and flow around the used design of the permanent magnets (**a**) and the magnetic field in the reactor (**b**).

3.3. Effects of Leaching Parameters on Fe Recovery from the Nonmagnetic Fraction Obtained by Conventional Magnetic Separation

Another method that can be used to enhance Fe recovery is double-magnetic separation. In the first stage of this method, the majority of the magnetite was recovered using conventional magnetic separation.

Evidently (Figure 12), the Fe recovery after the elimination of the majority of the magnetite by conventional magnetic separation was less dependent on the variations in the leaching parameters. The difference in the Fe recovery achieved at L:S ratios varying from 5 to 10 and T < 110 °C for a leaching time of 10–30 min did not exceed 4–6% (Figure 12a,b); this can be attributed to the higher ratio of the surface of the magnet to the magnetic concentrate. However, a temperature higher than 110 °C and the size fraction significantly influenced the Fe recovery. A high leaching temperature aids in increasing the dissolution of aluminosilicate, whereas an increase in the particle size results in a higher amount of aluminosilicate encapsulated in the magnetic spheres (Figure 9).

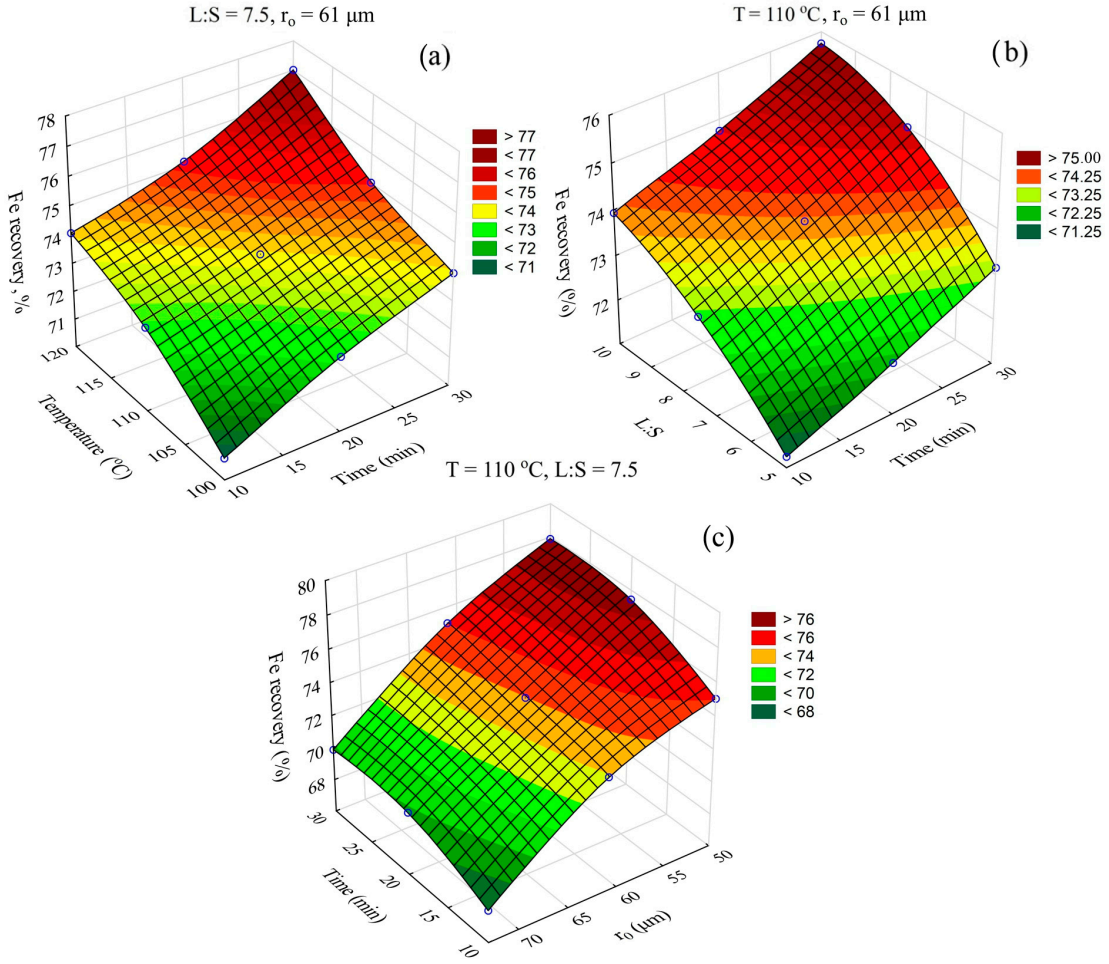

Figure 12. Neural network response surfaces for double-magnetic separation. The effect of: (**a**) time and temperature on the Fe recovery; (**b**) time and L:S ratio on the Fe recovery; (**c**) time and r_0 on the Fe recovery.

Considering the optimal conditions for desilication while maintaining a high silica extraction (>65%) and low co-extraction of aluminum (<10%), the Fe recovery achieved for the nonmagnetic fraction at T = 110 °C, t = 20 min, and L:S = 7.5 was 73.8%. The chemical compositions of the obtained desilicated coal fly ash (DCFA) and magnetic fraction are presented in Table 5. A comparison of the various Fe recovery methods using conventional wet magnetic separation before and after desilication at the optimal parameters is shown in Figure 13. As can be seen, the novel method of desilication with the simultaneous magnetic separation of the conventional non-magnetic fraction gave the best iron recovery efficiency.

Table 5. Chemical composition of the non-magnetic fraction obtained after the double-Fe separation process of the –50 µm particle size fraction of the raw CFA at T = 110 °C, τ = 20 min, and L:S = 7.5.

Product	Major Components (wt.%)									
	SiO_2	Al_2O_3	CaO	Fe_2O_3	TiO_2	MgO	Na_2O	K_2O	LOI	C
Desilicated CFA	36.17	44.30	3.40	1.83	1.85	0.86	0.92	0.08	7.30	2.67
Magnetic fraction	15.81	14.89	2.54	60.15	0.50	2.01	1.5	0.05	1.70	0.85

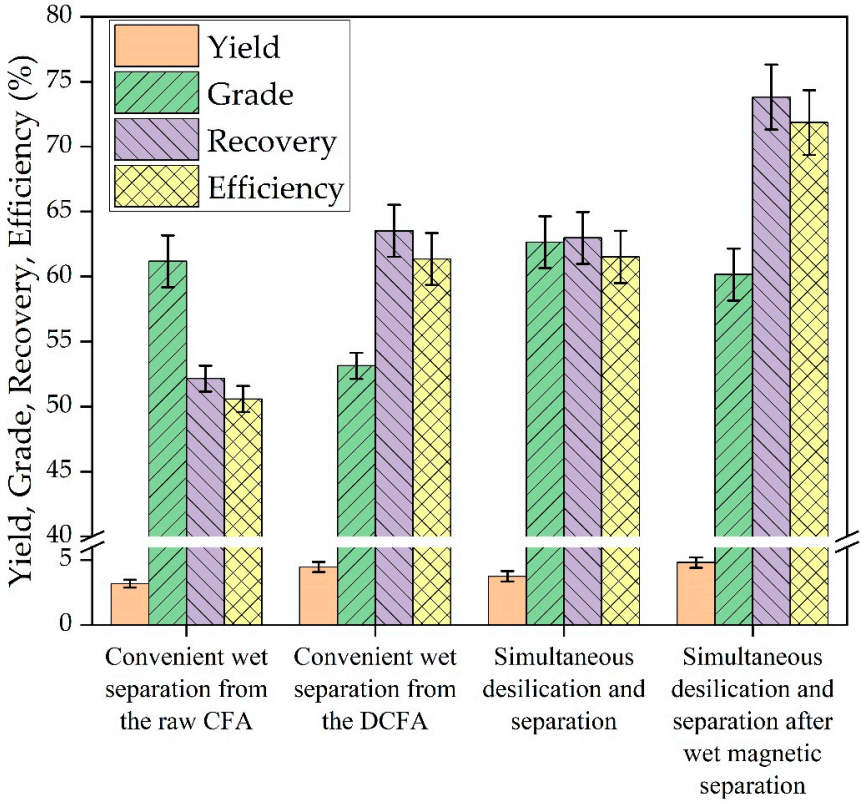

Figure 13. A comparison of the various Fe recovery methods' efficiency using conventional wet magnetic separation before and after desilication at the optimal parameters.

Figure 14 shows the magnetization measurements of the magnetic fraction obtained after the double-Fe separation (followed by simultaneous desilication and separation). Evidently, the magnetization reached a saturation value (Ms) of 25.6 emu g^{-1} at a magnetic field of 15 kOe. This value is lower than that of pure magnetite (60–90 emu g^{-1}), according to previous research [42,43]. This can be explained by the high amount of aluminosilicate that was co-extracted with the magnetite.

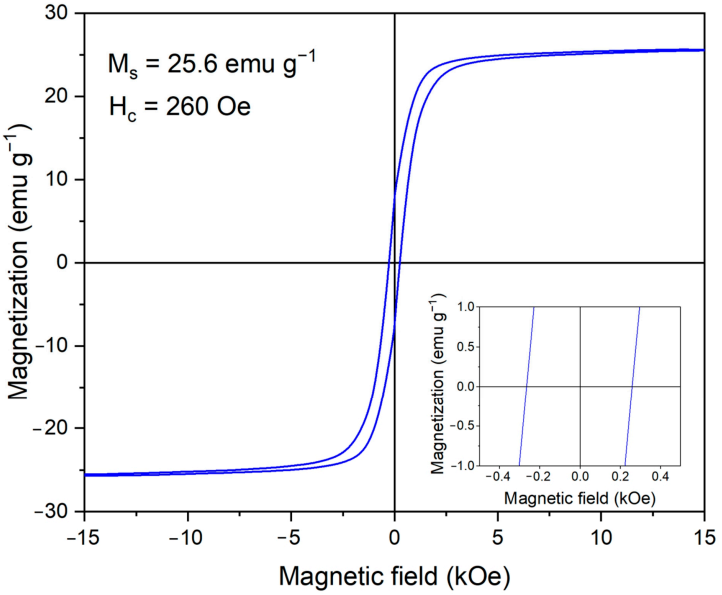

Figure 14. Magnetization curve for the magnetic fraction obtained after the double-Fe separation (followed by simultaneous desilication and separation).

Considering the obtained results, the following flowchart of CFA desilication with simultaneous iron recovery can be proposed (Figure 15).

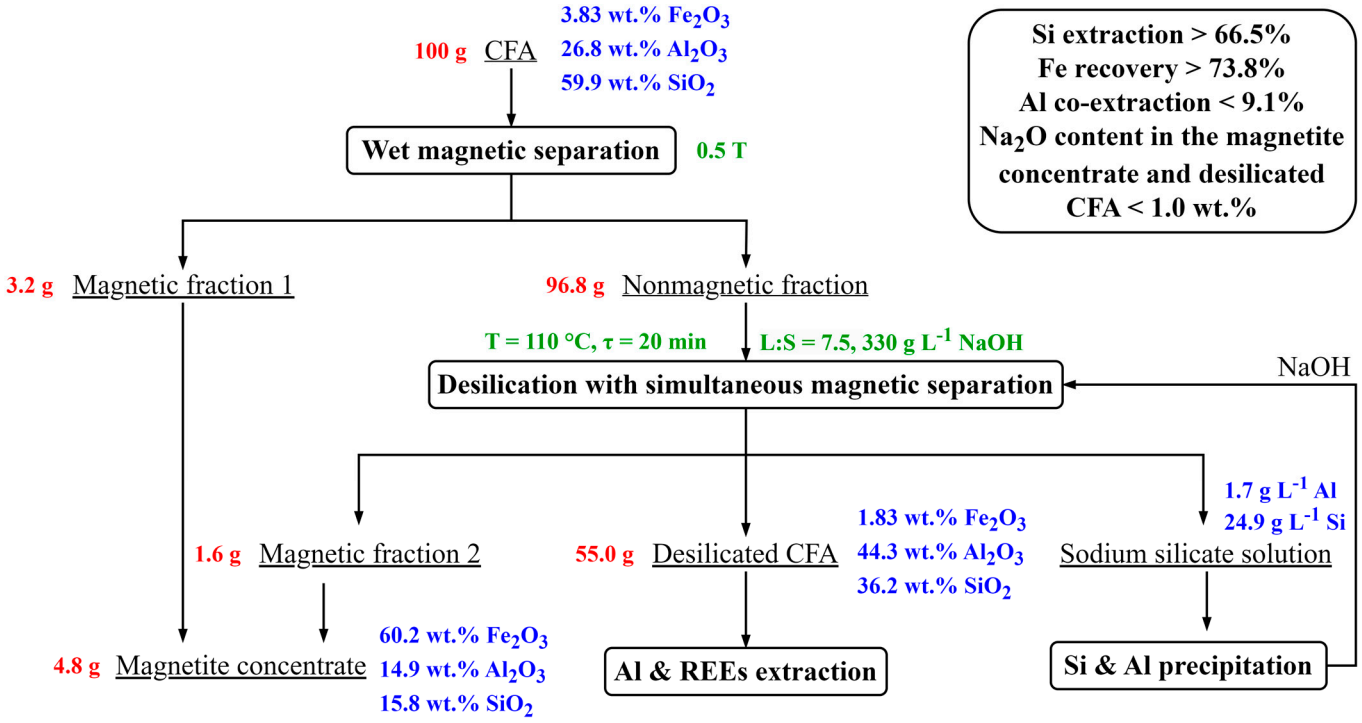

Figure 15. Flowsheet for the CFA desilication with the simultaneous iron recovery before Al and REE extraction.

4. Conclusions

CFA is a potential source for Al_2O_3 and REE extraction. However, this extraction is complicated by the presence of a large amount of amorphous glassy mass and iron, which results in a high amount of impurities in the pregnant solution and a lower extraction degree when hydrochemical processes are considered for extraction. Desilication and magnetic separation of CFA prior to leaching are common methods for CFA enrichment. However, the conventional desilication and magnetic separation methods result in a high Na_2O content in the Al and REE concentrates and a low-grade magnetic fraction.

In this study, a novel method was proposed for the complete dissolution of the amorphous glassy mass, with simultaneous magnetic separation. Evidently, the Fe recovery into the magnetic fraction could be significantly improved from 52% for raw CFA to 68% after desilication. After two stages of magnetic separation (wet magnetic separation followed by applying the novel method), the Fe recovery was increased to 73.8%. The effects of the leaching parameters (leaching duration, temperature (T, °C), L:S ratio, and initial particle size fraction) on the Al and Si extraction into a solution, the Fe recovery in the magnetic fraction, and the Na_2O content in the solid residue were evaluated. The leaching time and initial particle size were found to have a significant effect on the leaching efficiency. The SEM-EDX analysis revealed that a lower Fe recovery from the coarse particle size fraction was related to the encapsulation of the aluminosilicate in the magnetic sphere solid matrix. The optimal leaching parameters were determined as: temperature = 110 °C, L:S ratio = 7.5, leaching time 20 min. The extraction of the Si and Fe under these conditions was higher than 65% and 73%, respectively. The Al extraction and Na_2O contents in the solid residue were lower than 10% and 1 wt.%, respectively.

Author Contributions: Conceptualization, A.S. and I.L.; methodology, A.S. and L.C.; software, D.V.; validation, D.V. and J.P.; formal analysis, I.L. and J.P.; investigation, A.S. and L.C.; resources, A.S. and L.C.; data curation, A.S.; writing—original draft preparation, A.S. and D.V.; writing—review and editing, D.V. and J.P.; visualization, A.S.; supervision, I.L.; project administration, A.S.; funding acquisition, A.S. All authors have read and agreed to the published version of the manuscript.

Funding: This research was supported by the Russian Science Foundation and Government of Sverdlovsk region, Joint Grant No. 22-23-20150.

Data Availability Statement: All data are presented in this article.

Acknowledgments: The authors express their gratitude to Evgeny Kolesnikov from NUST MISiS for assistance in the SEM and XRD analyses of the solid samples.

Conflicts of Interest: The authors declare no conflict of interest.

References

1. Yu, X.; Cui, Y.; Chen, Y.; Chang, I.-S.; Wu, J. The Drivers of Collaborative Innovation of the Comprehensive Utilization Technologies of Coal Fly Ash in China: A Network Analysis. *Environ. Sci. Pollut. Res.* **2022**, *29*, 56291–56308. [CrossRef] [PubMed]
2. Liu, J.; Wang, Z.; Xie, G.; Li, Z.; Fan, X.; Zhang, W.; Xing, F.; Tang, L.; Ren, J. Resource Utilization of Municipal Solid Waste Incineration Fly Ash—Cement and Alkali-Activated Cementitious Materials: A Review. *Sci. Total Environ.* **2022**, *852*, 158254. [CrossRef]
3. Bhatt, A.; Priyadarshini, S.; Acharath Mohanakrishnan, A.; Abri, A.; Sattler, M.; Techapaphawit, S. Physical, Chemical, and Geotechnical Properties of Coal Fly Ash: A Global Review. *Case Stud. Constr. Mater.* **2019**, *11*, e00263. [CrossRef]
4. Kelechi, S.E.; Adamu, M.; Uche, O.A.U.; Okokpujie, I.P.; Ibrahim, Y.E.; Obianyo, I.I. A Comprehensive Review on Coal Fly Ash and Its Application in the Construction Industry. *Cogent Eng.* **2022**, *9*, 2114201. [CrossRef]
5. Sasui, S.; Kim, G.; Nam, J.; Koyama, T.; Chansomsak, S. Strength and Microstructure of Class-C Fly Ash and GGBS Blend Geopolymer Activated in NaOH & NaOH + Na_2SiO_3. *Materials* **2019**, *13*, 59. [CrossRef]
6. Finkelman, R.B.; Wolfe, A.; Hendryx, M.S. The Future Environmental and Health Impacts of Coal. *Energy Geosci.* **2021**, *2*, 99–112. [CrossRef]
7. Khan, I.; Umar, R. Environmental Risk Assessment of Coal Fly Ash on Soil and Groundwater Quality, Aligarh, India. *Groundw. Sustain. Dev.* **2019**, *8*, 346–357. [CrossRef]
8. Santamarina, J.C.; Torres-Cruz, L.A.; Bachus, R.C. Why Coal Ash and Tailings Dam Disasters Occur. *Science* **2019**, *364*, 526–528. [CrossRef]
9. Huang, S.; Ning, S.; Zhang, D.; Cai, Y.; Yan, X.; Liu, K.; Xu, X. Rare Earth Element Characteristics in Coal Ash from the Jungar Energy Gangue Power Plant, Inner Mongolia, China. *Minerals* **2023**, *13*, 1212. [CrossRef]
10. Bai, G.; Teng, W.; Wang, X.; Qin, J.; Xu, P.; Li, P. Alkali Desilicated Coal Fly Ash as Substitute of Bauxite in Lime-Soda Sintering Process for Aluminum Production. *Trans. Nonferrous Met. Soc. China* **2010**, *20*, s169–s175. [CrossRef]
11. Blissett, R.S.; Rowson, N.A. A Review of the Multi-Component Utilisation of Coal Fly Ash. *Fuel* **2012**, *97*, 1–23. [CrossRef]
12. Shoppert, A.; Valeev, D.; Napol'skikh, J.; Loginova, I.; Pan, J.; Chen, H.; Zhang, L. Rare-Earth Elements Extraction from Low-Alkali Desilicated Coal Fly Ash by $(NH_4)_2SO_4$ + H_2SO_4. *Materials* **2023**, *16*, 6. [CrossRef] [PubMed]
13. Smith, P. The Processing of High Silica Bauxites—Review of Existing and Potential Processes. *Hydrometallurgy* **2009**, *98*, 162–176. [CrossRef]
14. Apua, M.C.; Nkazi, B.D. Leaching of Coal Fly Ash with Sulphuric Acid for Synthesis of Wastewater Treatment Composite Coagulant. *Can. Metall. Q.* **2022**, *61*, 309–331. [CrossRef]
15. Guo, Y.; Zhao, Z.; Zhao, Q.; Cheng, F. Novel Process of Alumina Extraction from Coal Fly Ash by Pre-Desilicating—Na2CO3 Activation—Acid Leaching Technique. *Hydrometallurgy* **2017**, *169*, 418–425. [CrossRef]
16. Tripathy, A.K.; Behera, B.; Aishvarya, V.; Sheik, A.R.; Dash, B.; Sarangi, C.K.; Tripathy, B.C.; Sanjay, K.; Bhattacharya, I.N. Sodium Fluoride Assisted Acid Leaching of Coal Fly Ash for the Extraction of Alumina. *Miner. Eng.* **2019**, *131*, 140–145. [CrossRef]
17. Li, X.; Ma, B.; Wang, C.; Chen, Y.; Yang, W.; Zhang, W. A Sustainable Process to Recycle Aluminum from Coal Fly Ash for Simultaneous Removal of Iron: Solid Waste Management and Evaluation. *Miner. Eng.* **2022**, *184*, 107638. [CrossRef]
18. Zong, Y.; Li, F.; Chen, W.; Liu, Z. Extraction of Alumina from High-Alumina Coal Ash Using an Alkaline Hydrothermal Method. *SN Appl. Sci.* **2019**, *1*, 783. [CrossRef]
19. Li, S.; Bo, P.; Kang, L.; Guo, H.; Gao, W.; Qin, S. Activation Pretreatment and Leaching Process of High-Alumina Coal Fly Ash to Extract Lithium and Aluminum. *Metals* **2020**, *10*, 893. [CrossRef]
20. Li, X.; Wang, H.; Zhou, Q.; Qi, T.; Liu, G.; Peng, Z. Efficient Separation of Silica and Alumina in Simulated CFB Slag by Reduction Roasting-Alkaline Leaching Process. *Waste Manag.* **2019**, *87*, 798–804. [CrossRef]
21. Yan, L.; Shang, J.; Wang, Y.; Li, J.; Liu, H.; Qu, T.; Zhang, C. Experimental Parameter Optimization Study on the Acid Leaching of Coal Fly Ash. *Desalination Water Treat.* **2016**, *57*, 10894–10904. [CrossRef]
22. Shoppert, A.; Valeev, D.; Loginova, I.; Chaikin, L. Complete Extraction of Amorphous Aluminosilicate from Coal Fly Ash by Alkali Leaching under Atmospheric Pressure. *Metals* **2020**, *10*, 1684. [CrossRef]

23. Pan, J.; Long, X.; Zhang, L.; Shoppert, A.; Valeev, D.; Zhou, C.; Liu, X. The Discrepancy between Coal Ash from Muffle, Circulating Fluidized Bed (CFB), and Pulverized Coal (PC) Furnaces, with a Focus on the Recovery of Iron and Rare Earth Elements. *Materials* **2022**, *15*, 8494. [CrossRef]
24. Fan, X.; Xia, J.; Zhang, D.; Nie, Z.; Liu, Y.; Zhang, L.; Zhang, D. Highly-Efficient and Sequential Recovery of Rare Earth Elements, Alumina and Silica from Coal Fly Ash via a Novel Recyclable ZnO Sinter Method. *J. Hazard. Mater.* **2022**, *437*, 129308. [CrossRef]
25. Li, Q.; Ji, B.; Xiao, Z.; Zhang, W. Alkali Pretreatment Effects on Acid Leaching Recovery of Rare Earth Elements from Coal Waste of the Western Kentucky No. 13 and Fire Clay Seams. *Min. Min. Mater.* **2022**, *1*, 7. [CrossRef]
26. Wu, G.; Wang, T.; Chen, G.; Shen, Z.; Pan, W.-P. Coal Fly Ash Activated by NaOH Roasting: Rare Earth Elements Recovery and Harmful Trace Elements Migration. *Fuel* **2022**, *324*, 124515. [CrossRef]
27. Gong, Y.; Sun, J.; Sun, S.-Y.; Lu, G.; Zhang, T.-A. Enhanced Desilication of High Alumina Fly Ash by Combining Physical and Chemical Activation. *Metals* **2019**, *9*, 411. [CrossRef]
28. Aphane, M.E.; Doucet, F.J.; Kruger, R.A.; Petrik, L.; van der Merwe, E.M. Preparation of Sodium Silicate Solutions and Silica Nanoparticles from South African Coal Fly Ash. *Waste Biomass Valor.* **2019**, *11*, 4403–4417. [CrossRef]
29. Ma, Z.; Zhang, X.; Guo, Y.; Cheng, F. Extraction of Valuable Metals and Preparation of Mesoporous Materials from Circulating Fluidized Bed-Derived Fly Ash via an Acid–Alkali-Based Alternate Method. *ACS Omega* **2020**, *5*, 31295–31305. [CrossRef]
30. Ma, Z.; Zhang, S.; Zhang, H.; Cheng, F. Novel Extraction of Valuable Metals from Circulating Fluidized Bed-Derived High-Alumina Fly Ash by Acid–Alkali–Based Alternate Method. *J. Clean. Prod.* **2019**, *230*, 302–313. [CrossRef]
31. Nugroho, N.D.; Rosita, W.; Perdana, I.; Bendiyasa, I.M.; Mufakhir, F.R.; Astuti, W. Iron Bearing Oxide Minerals Separation from Rare Earth Elements (REE) Rich Coal Fly Ash. *IOP Conf. Ser. Mater. Sci. Eng.* **2019**, *478*, 012026. [CrossRef]
32. Shi, Y.; Jiang, K.; Zhang, T.; Zhu, X. Simultaneous Separation of Fe & Al and Extraction of Fe from Waste Coal Fly Ash: Altering the Charge Sequence of Ions by Electrolysis. *Waste Manag.* **2022**, *137*, 50–60. [CrossRef]
33. Fu, B.; Hower, J.C.; Zhang, W.; Luo, G.; Hu, H.; Yao, H. A Review of Rare Earth Elements and Yttrium in Coal Ash: Content, Modes of Occurrences, Combustion Behavior, and Extraction Methods. *Prog. Energy Combust. Sci.* **2022**, *88*, 100954. [CrossRef]
34. Trinh, H.B.; Kim, S.; Lee, J. Recovery of Rare Earth Elements from Coal Fly Ash Using Enrichment by Sodium Hydroxide Leaching and Dissolution by Hydrochloric Acid. *Geosystem Eng.* **2022**, *25*, 53–62. [CrossRef]
35. Rosita, W.; Bendiyasa, I.M.; Perdana, I.; Anggara, F. Sequential Particle-Size and Magnetic Separation for Enrichment of Rare-Earth Elements and Yttrium in Indonesia Coal Fly Ash. *J. Environ. Chem. Eng.* **2020**, *8*, 103575. [CrossRef]
36. Zhou, C.; Li, C.; Li, W.; Sun, J.; Li, Q.; Wu, W.; Liu, G. Distribution and Preconcentration of Critical Elements from Coal Fly Ash by Integrated Physical Separations. *Int. J. Coal Geol.* **2022**, *261*, 104095. [CrossRef]
37. Zinoveev, D.V.; Delicyn, L.M.; Ryabov, Y.V.; Kulumbegov, R.V.; Zakunov, A.S.; Dyubanov, V.G. Magnetite Concentrate from Coal Fly Ash of Kashirskaya GRES- the Raw Material for the Production of Metal Products by Reduction Smelting. *J. Phys. Conf. Ser.* **2021**, *1942*, 012048. [CrossRef]
38. Sommerville, R.; Blissett, R.; Rowson, N.; Blackburn, S. Producing a Synthetic Zeolite from Improved Fly Ash Residue. *Int. J. Miner. Process.* **2013**, *124*, 20–25. [CrossRef]
39. Vasilyev, A.M.; Kuskov, V.B. Specific Features of the Concentration Process for Fine-Grained Materials in a Short-Cone Hydrocyclone. *Obogashchenie Rud* **2018**, *2*, 30–34. [CrossRef]
40. Kanarskii, A.V.; Adamov, E.V.; Krylova, L.N. Flotation Concentration of the Sulfide Antimony-Arsenic Gold-Bearing Ore. *Russ. J. Non-Ferr. Met.* **2012**, *53*, 120–124. [CrossRef]
41. Valeev, D.; Bobylev, P.; Osokin, N.; Zolotova, I.; Rodionov, I.; Salazar-Concha, C.; Verichev, K. A Review of the Alumina Production from Coal Fly Ash, with a Focus in Russia. *J. Clean. Prod.* **2022**, *363*, 132360. [CrossRef]
42. Shoppert, A.; Valeev, D.; Diallo, M.M.; Loginova, I.; Beavogui, M.C.; Rakhmonov, A.; Ovchenkov, Y.; Pankratov, D. High-Iron Bauxite Residue (Red Mud) Valorization Using Hydrochemical Conversion of Goethite to Magnetite. *Materials* **2022**, *15*, 8423. [CrossRef] [PubMed]
43. Tuutijärvi, T.; Lu, J.; Sillanpää, M.; Chen, G. As(V) Adsorption on Maghemite Nanoparticles. *J. Hazard. Mater.* **2009**, *166*, 1415–1420. [CrossRef] [PubMed]